Lessons Learned from Large-Scale Aerospace Structural Testing

Andrew E. Lovejoy,* Dawn C. Jegley,† Mark W. Hilburger,‡ and Adam Przekop§
NASA Langley Research Center, Hampton, Virginia 23681

Large-scale testing of aerospace structures is frequently the final step in a development project to validate the structural performance, and that step typically involves a large cost and time investment. To ensure that the testing provides the required data, avoiding errors that can result in an unsuccessful test and failure to meet objectives is critical. Five lessons learned are presented herein to provide insight to those conducting large-scale tests to help them avoid known pitfalls that may result in an unsuccessful test. Five large-scale tests are described, and they include two composite wing tests, a full-scale 27.5-ft-diam metallic barrel test, an 8-ft-diam metallic barrel test, and a composite hybrid-wing–body center section test. Problems identified during the testing and mitigation approaches to solve the problems are presented, and then the lessons learned are identified and discussed.

I. Introduction

LARGE-SCALE testing of representative aerospace structures is used to validate the performance of the structures or to provide full-scale response characteristics for validation of analysis methods. Whenever possible, a building-block test program is used for large-scale testing, where a full-scale test is the culmination of years of research to demonstrate the performance of the final design. In other cases, the full-scale test is used when the proper full-scale response cannot easily be represented by subscale testing, which is particularly true for composite structures where scaled testing is typically not easily accomplished. In either case, these large-scale tests represent significant investment in terms of cost and time, and having a successful test is of utmost importance. Lessons learned by researchers at the NASA Langley Research Center (LaRC) from large-scale structural testing conducted at LaRC, NASA Marshall Space Flight Center (MSFC), and NASA Armstrong Flight Research Center (AFRC) are presented in this paper. The test articles examined to provide lessons learned are the Advanced Composites Technology (ACT) program full-scale 40-ft-long semispan stitched composite wing (SCW) [1]; the Advanced Air Transport Technology (AATT) project 39-ft-long, 27%-scale tow-steered passive aeroelastic tailored (PAT) wing [2]; the Shell Buckling Knockdown Factor (SBKF) project full-scale 27.5-ft-diam metallic barrels [3]; the SBKF large-scale 8-ft-diam metallic barrels [4]; and the stitched composite Environmentally Responsible Aircraft (ERA) project, 80%-scale multibay box (MBB) representative of the center section of a hybrid-wing–body (HWB) aircraft [5]. Descriptions of the test articles and the testing conducted, descriptions of problems identified during the testing, definitions of developed mitigation approaches to solve the problems, and lessons learned are identified and discussed in the following sections of this paper.

II. Large-Scale Tests

Lessons learned that will be discussed herein are taken from five large-scale structural tests of aerospace components. Three of the tests are of composite structures, namely, the SCW (Sec. II.A), the

PAT wing (Sec. II.B), and the MBB (Sec. II.C). The other two test articles are from the SBKF large-scale metallic barrel tests, namely, the 27.5-ft-diam full-scale (Sec. II.D) and the 8-ft-diam large-scale test articles (Sec. II.E). Descriptions and details of these tests are presented in the remainder of this section.

A. Stitched Composite Wing

The full-scale 40-ft-long SCW was a carbon fiber/epoxy, resin-infused test article with through-the-thickness stitches to replace fasteners and to suppress damage growth, and was representative of a wing for a 200-passenger commercial transport aircraft. The SCW consisted primarily of the upper and lower covers, leading and trailing edge spars, and 18 ribs. The SCW test setup is shown in Fig. 1. The test article was attached to the strongback at LaRC using a set of metallic mounting plates that were attached around the perimeter of the test article root region, including the upper and lower covers and the leading and trailing edge spars, to provide a clamped condition. The upper and lower covers were of unitized construction with the skin, stringers, and intercostals all stitched together. The stitching was applied in a uniform manner throughout the entirety of the upper and lower cover skins and the stringers to suppress damage growth (i.e., uniform stitch length and stitch spacing in the entire structure). The leading and trailing edge spars and the ribs were mechanically fastened to the upper and lower covers, and the ribs were also mechanically fastened to the spars. Loads were introduced into the test article using a total of nine hydraulic actuated load lines. These load lines were mounted to the floor at I-beam locations embedded in the concrete floor. Pairs of actuators were located at four spanwise locations, with one actuator at the leading edge (LE) and one actuator at the trailing edge (TE) at each spanwise location. The pair of actuators at the tip was attached to a metallic closeout rib/fixture (Fig. 1), the actuator pair immediately inboard of the tip was attached to a saddle that encapsulated the test article (Fig. 1), and the remaining two pairs of actuators closest to the wing root were attached to local fittings connected to the spars. Therefore, for the $-1g$ down-bending and $2.5g$ up-bending load cases, the SWC was clamped to the strongback and had eight loads applied. For the third load case, braked roll (aborted takeoff ground roll with maximum breaking and full fuel load), an additional line load was added using the load arm shown in Fig. 1. The load arm was attached to an I-beam connected to plates mounted on the upper and lower covers, and extended downward behind the wing to be loaded by the ninth actuator attached to the floor to apply a landing gear attachment force. A detailed description of the test article, setup, and testing is provided in Ref. [1].

B. Passive Aeroelastic Tailored Wing

The 39-ft-long, subscale tow-steered PAT wing was a carbon fiber/epoxy wing [2] based on a variant of the NASA Common Research Model [6] that is representative of a wide-body commercial transport aircraft. The PAT wing included upper and lower skins, leading and trailing edge spars, and 58 ribs [7]. Both skins of the PAT wing were

*Research Aerospace Engineer, Structural Mechanics and Concepts Branch; andrew.e.lovejoy@nasa.gov; Associate Fellow AIAA (Corresponding Author).

†Research Aerospace Engineer, Structural Mechanics and Concepts Branch. Associate Fellow AIAA.

‡Principal Technologist for Structures, Materials, and Nanotechnology, Space Technology Mission Directorate. Associate Fellow AIAA.

§Supervisory Research Aerospace Engineer, Structural Mechanics and Concepts Branch. Associate Fellow AIAA.
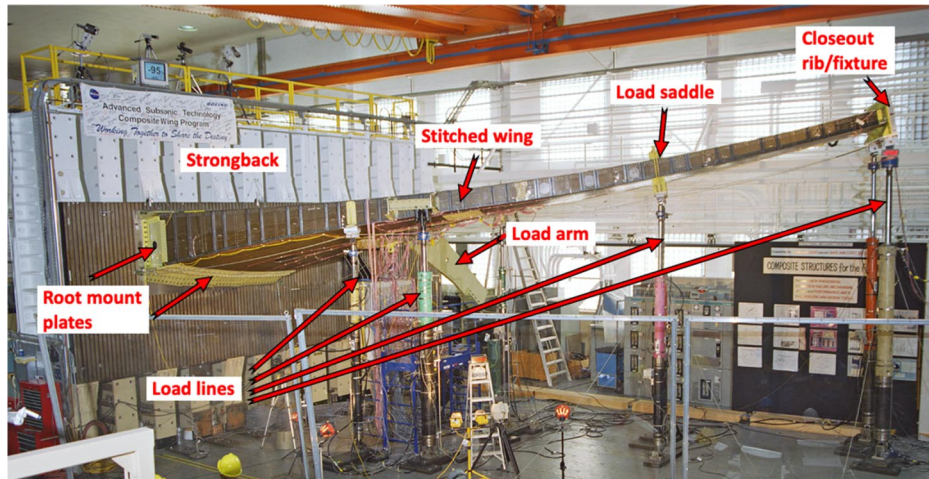
Fig. 1   SCW test setup.

fabricated using tow-steered composites, while the spars and ribs were fabricated using conventional composite laminates. Due to numerous manufacturing flaws, including delaminations and wrinkling, the outboard 11 ft of the leading-edge composite spar was replaced with an aluminum spar section of nearly equivalent size and performance. The PAT wing test setup at AFRC is shown in Fig. 2. The wing was mounted to two root reaction plates that were connected to the leading and trailing edge spars using four 3-in.-diam attachment pins, two in each spar as shown for clarity in a schematic of the PAT wing test setup in Fig. 3. The root reaction plates were connected to a 6-degree-of-freedom reaction table using angle brackets, with the reaction table supported by load cells at six locations atop a base pedestal (Fig. 3). The pedestal was joined to three steel support I-beams that were connected to the load lines, completing a self-reacting test system. Load was applied using seven pairs of load-introduction points at seven spanwise (rib) locations, with one loading point at the LE spar and one loading point at the TE spar at each spanwise location (Fig. 3). Load line pairs were sequentially numbered 1–7, with location 1 closest to the root and location 7 at the wing tip. For the $-1g$ down-bending load condition and the flex axis testing, load lines were attached to the test article and support I-beams for locations 1 through 6, but at location 7 (the wing tip) the load lines were attached to the test article and floor because the wing tip extended past the support I-beams. Load lines for the $-1g$ down-bending are shown in black in Fig. 3. For the $2.5g$ up-bending load condition, the outboard three sets of load locations (5, 6, and 7) were

connected to the overhead load structure identified in Fig. 3, with the steel overhead load structure connected to the support I-beams to retain a self-reacting system. The pairs of wing loads at each outboard station were applied using a single loading actuator for each of the load stations, with the three loading actuators embedded in the overhead load structure. Cables connected the loading actuators to the corresponding pairs of wing load connection points at each of the three spanwise loading locations. The cables were guided by movable pulleys that enabled control of the loading direction at each location. The cables were attached to I-beams that split the load to the two wing connection points (LE and TE) in a whiffle tree configuration as seen in Fig. 3, with the positioning of each overhead cable connection to the whiffle tree I-beams providing the correct load division between the corresponding two wing connection points. Load lines for the $2.5g$ up-bending condition are shown in red in Fig. 3. A detailed description of the test article, setup, and testing is provided in Ref. [2].

C.   SBKF 27.5-ft-Diam Metallic Barrels

Two full-scale 27.5-ft-diam metallic barrel test articles, designated External Tank derived Test Article 1 (ETTA1) and 2 (ETTA2), were fabricated at MSFC from eight existing Space Shuttle external tank (ET) panels for tests at MSFC in support of an effort to update the buckling-critical launch vehicle structure buckling knockdown factors. The panels used to fabricate the ETTA1 and ETTA2 barrels were manufactured from Al-Li-2195 flat plate material stock, into which an
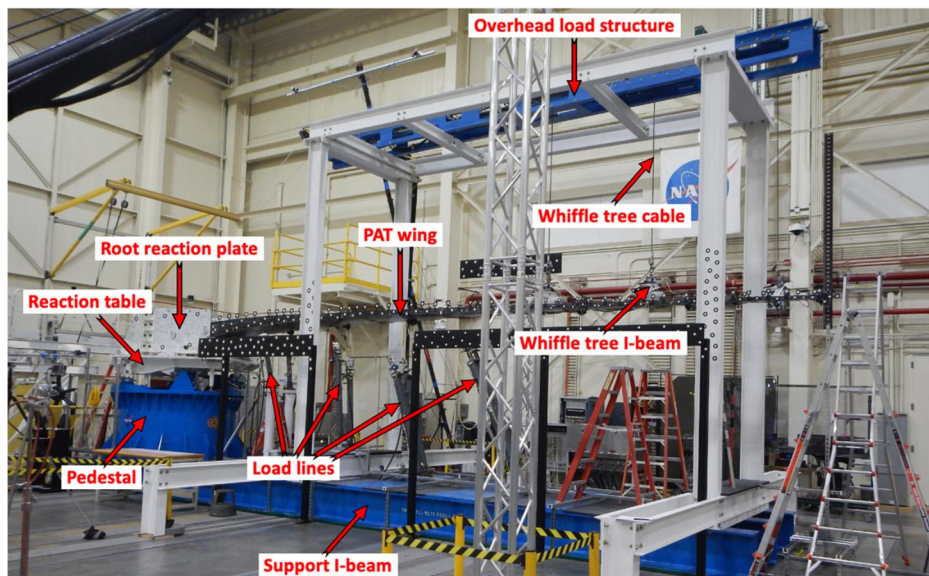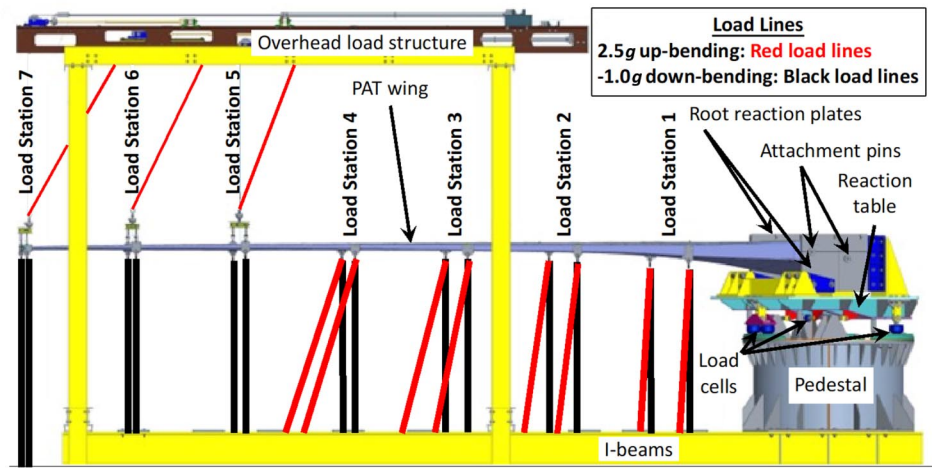

Fig. 2   PAT wing test setup.

Fig. 3   Schematic of PAT wing test setup.

orthogrid stiffener pattern was machined to form skin pockets and weld land details. The flat orthogrid panels were then bump-formed to an outer mold line (OML) radius of 168.0 in. and then heat-treated to their final temper (i.e., the panels were underformed relative to the final cylinder OML radius of 165.5 in.). Eight curved orthogrid panels were then friction-stir welded together using a vertical weld tool at MSFC to construct each complete 20-ft-tall cylindrical ETTA barrel. The test setup for the SBKF full-scale testing is shown in Fig. 4. The test configuration comprises the load test annex (LTA) crosshead at the top of the setup to which eight hydraulic load lines were connected, an upper load-introduction cylinder (comprising the liquid oxygen [LO2] tank load introduction ring and simulator) to which the load lines were attached, the test article and attachment rings, and the lower load-introduction cylinder (comprising the liquid hydrogen [LH2] tank load introduction ring and simulator) that was connected to the LTA floor at the bottom of the test setup (Fig. 4). The nearly 70-ft "stack" comprised the components between the LTA floor and crosshead and included the LH2 load ring at the bottom through the load lines at the top. The LTA crosshead and floor constitute rigid boundaries (i.e., ground locations). The upper and lower load-introduction cylinders were heritage hardware for which there was limited design information. Test loading consisted of various combinations of axial compression, bending, and internal pressure. The test system loads were limited by the capacity of the hydraulic load actuators, which were limited to 2.25 million pounds of axial compression, and 1.4 psi

internal pressure. A detailed description of the test article, setup, and testing is provided in Ref. [3].

D.   SBKF 8-ft-Diam Metallic Barrels

As part of the SBKF project, eight subscale metallic barrels were designed and tested. These subscale barrels were large-scale 8-ft-diam barrels that were designed to have response characteristics similar to large-scale launch vehicle cylindrical structures such as those used in the NASA Space Launch System (SLS) heavy-lift launch vehicle [8]. Machined integral orthogrid and isogrid stiffener patterns were used, and each barrel consisted of three Al-Li-2195 panels that were machined flat and then bump formed into the 4-ft radius. Three panels were friction stir welded to form each of the completed test articles.

Testing was conducted at MSFC using the test assembly shown in Fig. 5, which was designed, analytically verified, and fabricated to meet program test objectives (e.g., boundary conditions, such as restraining the rotation of the test barrel at the ends). The test assembly was a self-reacting load system (termed the stack) that comprised an upper and lower load spider, 16 load struts, upper and lower transition cylinders, the test article assembly, and 8 load lines. Each load line was connected to the top and bottom load spiders and consisted of a hydraulic cylinder, a 4-in.-diam loading rod, a load cell, and attachment hardware. The load lines could be controlled independently in load control or stroke (position) control to apply uniform compression or
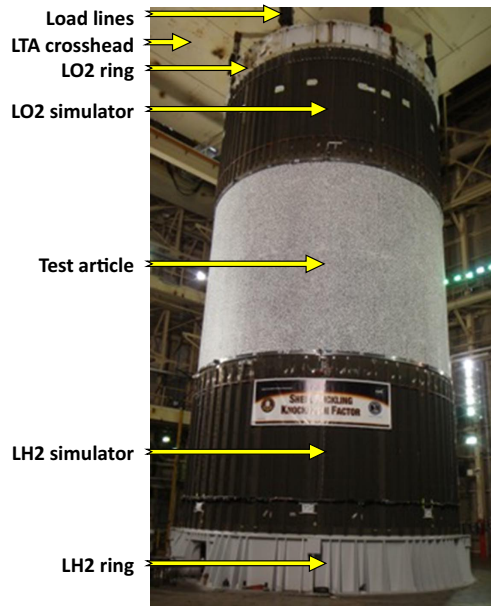

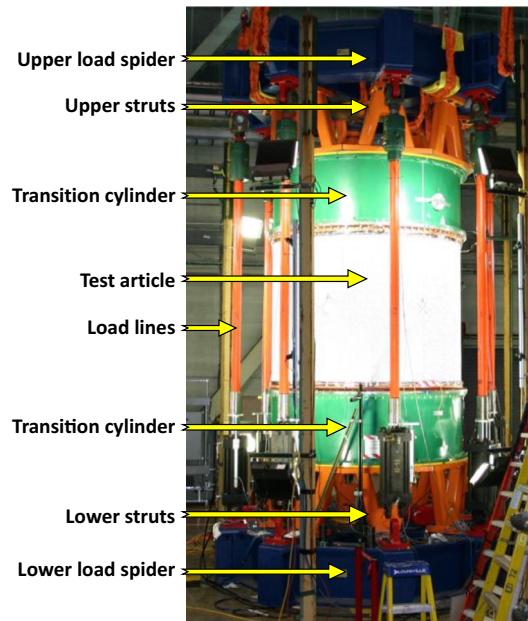**Fig. 4   SBKF full-scale metallic barrel test setup.**

Fig. 5   SBKF 8-ft-diam metallic barrel test setup.

combined compression and bending with a maximum load capability of 1.5 million pounds of axial compression force and 80,000 pounds of axial tension. The test articles were attached to upper and lower load rings using a low-temperature-melting-point metallic grout and bolts before being installed in the stack. During the testing process for the load conditions of axial load, bending load, and combined axial and bending load, the weight of the upper part of the assembly (transition cylinder and spider) was removed from the test article in a tare procedure so that testing began with zero loads applied to the test article. A detailed description of the test article, setup, and testing is provided in Ref. [4].

E. Multibay Box

The MBB test article was a stitched, resin-infused carbon fiber structure that was 30 ft long, 14 ft tall, and 7 ft deep, and represented an 80%-scale section of the most heavily loaded center region of the HWB configuration. The MBB, shown mounted between the platens in the LaRC Combined Loads Test System (COLTS) in Fig. 6, contained 11 pultruded rod-stitched efficient unitized structure (PRSEUS) panels that formed the exterior shell and floor members, and four interior sandwich rib panels that were used to divide the box width into thirds. In a HWB aircraft, the bulkheads would be near the cockpit and near the tail, while in the test article they are only 7 ft apart. The test article was designed so that these bulkheads would support the same type of loading as would be found in the actual aircraft. Load conditions consisted of mechanical load only that represented $-1g$ down-bending and $2.5g$ up-bending aerodynamic loads, internal pressure load only, and combined mechanical and internal pressure load. Load-introduction boxes (attach fittings) were added to the test article to mate with the COLTS platens to ensure that load was introduced into the test article in such a way as to avoid failure at the outer rib locations [5], as shown in the schematic in Fig. 7. Loads were applied by four load lines attached to the reaction and moving platens as shown in Fig. 7. The reaction platen was stationary but was able to rotate when bending loads were applied (e.g., the top rotated toward the moving platen and the bottom rotated away from the moving platen for up-bending). The moving platen was free to move based on the applied loads. Air for internal pressure load was introduced into the bottom section of the MBB. Holes in the floor separating the top and bottom sections permitted the air to equalize pressure throughout the MBB. A detailed description of the test article, setup, and testing is presented in Ref. [5].

III. Lessons Learned

The five large-scale tests presented in the previous section yielded five lessons learned that are associated with test analysis, test design, instrumentation, and load introduction. Lessons are presented herein
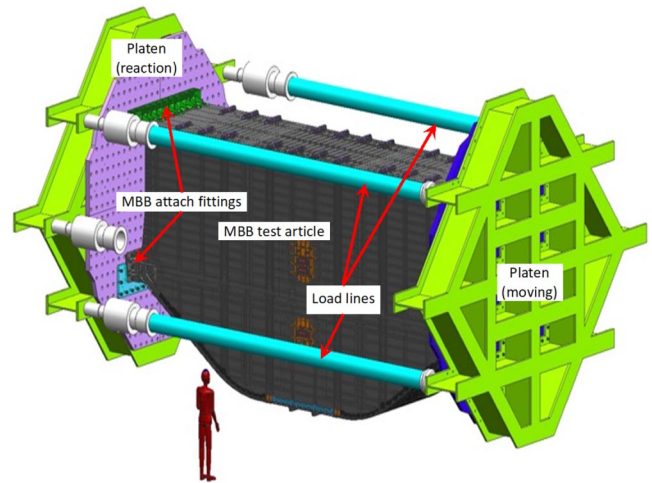

Fig. 7 Schematic of COLTS MBB test setup.

by first describing the observed response for various tests, and then describing how the data were handled or what measures were taken to mitigate the problem.

A. Lesson 1: Test Analysis

The first lesson learned is associated with test analysis. Both the SCW and the PAT wing tests had similar challenges that led to an important lesson learned. Often, a test is intended to demonstrate the ability of the structure to satisfy a set of design requirements and sustain required loads. Tests to demonstrate satisfaction of requirements are designed with the intent that actual operational loads are applied during the test, thereby resulting in the correct load distribution within the structure. Applied loading on these two wing test articles was intended to represent specific loads that would be experienced by the wings during service. The SCW test was designed to apply aerodynamic load conditions of $-1g$ down-bending, $2.5g$ up-bending, and braked roll load conditions, and the PAT wing test was designed to apply aerodynamic load conditions of $-1g$ down-bending and $2.5g$ up-bending. Preliminary analyses and test design were carried out using linear static analysis for each load condition. However, geometrically nonlinear analysis was carried out before testing because it was necessary to capture the anticipated test response due to the large deflections. Nonlinear static analyses were conducted for both test articles, and the first sets of nonlinear analyses were carried out with the loads applied at the actuator connection
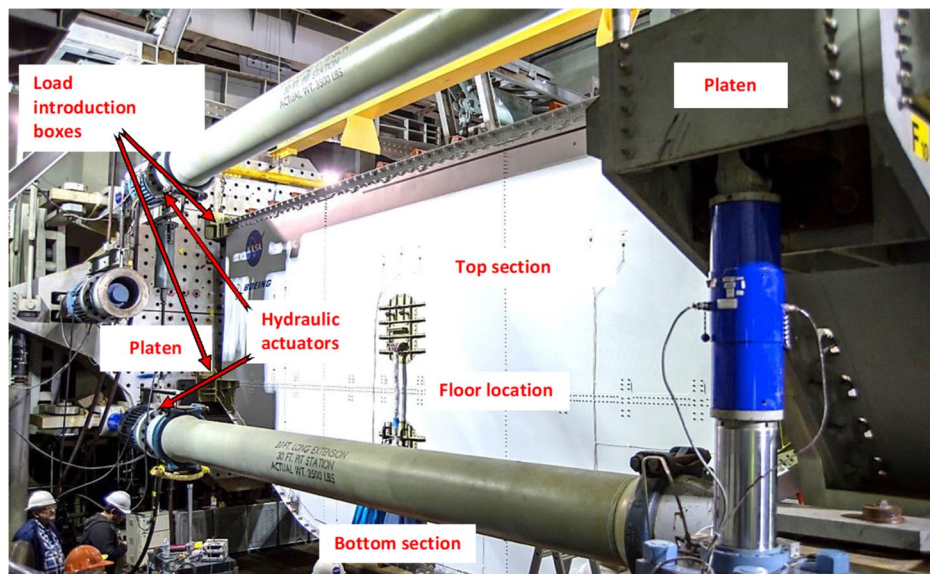

Fig. 6 MBB test setup.

points as follower loads because that was more representative of the aerodynamic loads on the real wing. However, as seen in Figs. 1 and 2, there were conventional load lines that were connected to the test article at one end and at a fixed point on the other. During testing, the applied test loads remained aligned with the load lines and were not follower forces with respect to the test article as would be expected for the aerodynamic loads on the real wing.

Failure to initially model the test load conditions accurately resulted in deficiencies with the original test configuration fixture designs. For the SCW, the analyses with applied loads modeled as follower loads with respect to the test article meant that the modeled loads at the tip remained in the plane of the metallic closeout rib/fixture. As a result, only in-plane forces were predicted to exist in the metallic rib/fixture. However, as seen in Fig. 1, the load lines did not remain coplanar with the closeout rib/fixture during test. During the experimental load application, the forces in the test remained aligned with respect to the load line orientation and not the test article and fixtures; therefore, analyses were updated to keep the load aligned with the load line. The finite element model (FEM) is shown in Fig. 8 with the outboard two sets of load lines and fixtures explicitly modeled before testing, allowing for modifications to the test setup. By including beam representations of the load lines and defining the loads as follower loads with respect to those beams, the modified FEM better represented the test condition. This improved FEM was used to accurately capture the test load orientations that resulted in a combination of in-plane and normal forces on the closeout rib/fixture at the tip of the SCW test article. The initial design of this closeout rib/fixture was an unstiffened thick metallic plate. The normal force predicted upon applying the loads consistent with the test configuration resulted in predicted bending stresses sufficient for the metallic closeout rib/fixture to yield. Therefore, as seen in Figs. 1 and 8, stiffeners were added to the closeout rib/fixture to alleviate the predicted bending that led to the potential yielding behavior. As a result of the experience with the SCW, similar load lines for the PAT wing were installed at an angle, as shown in Fig. 3, so that at the maximum

applied test load, the load line would apply load as close to normal to the wing as possible to better represent the aerodynamic loads at maximum load.

Another loading concern that arose in both the SCW and PAT wing tests was response due to eccentric loading. For the SCW, the load arm for the braked roll condition was eccentric from the I-beam extending off the back of the test article because the load arm was mounted on one side of the I-beam. That eccentricity was not included in initial test design analyses. When the eccentricity was included in the analysis model and nonlinear analysis was performed, the load arm was predicted to bend during the test. A mitigation strategy was developed that incorporated an additional load line connected between the strongback and the load arm. The added load line restrained the motion of the load arm adjacent to the braked roll actuator so that the load arm remained nearly in-plane during testing, as was desired. The deflection contours are shown in Fig. 9 for the load arm where the out-of-plane displacement at the braked roll actuator end was reduced from almost 3.5 in. to about 0.2 in, a reduction of displacement of around 95% [9], where the connection point of the load arm side control actuator is indicated by the red dot in Fig. 9b. Using the experience from the SCW regarding load eccentricity, the first author identified a similar issue with the PAT wing, where the load lugs to which the load lines were attached were initially modeled with the load applied to the center of the connection pin hole in the plane of the load lug (zero eccentricity). However, the load line was actually connected to one side of the load lug for the test resulting in an eccentric load as shown in Fig. 10a. When the eccentricity was included in the final pretest analysis model and nonlinear analysis conducted, excessive bending stresses were predicted that created significant negative margins in several of the lugs. The mitigation was to manufacture couplers so that the load line was attached below the load lug to eliminate the eccentricity and to keep the applied load in the plane of the load lug as shown in Fig. 10b. These examples demonstrate the first lesson learned:
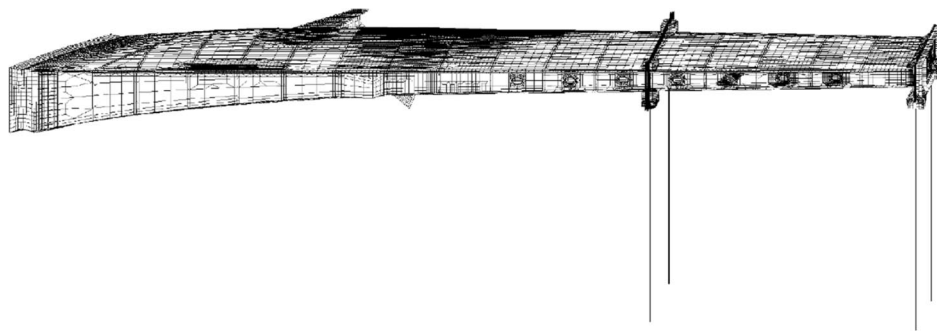
Fig. 8   SCW FEM with outboard load lines and fixturing explicitly modeled (from Ref. [1]).

a) Original design

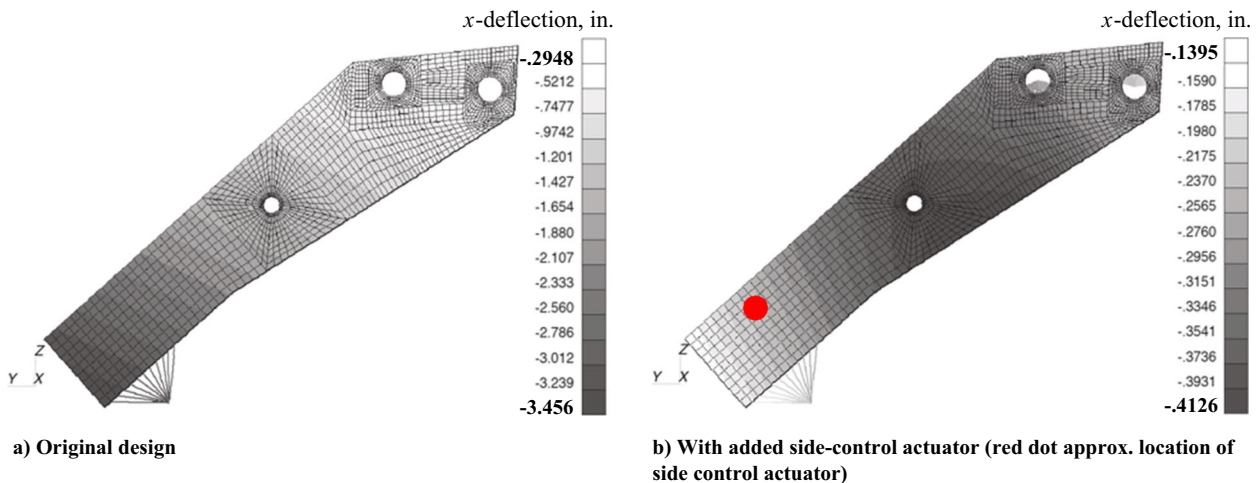b) With added side-control actuator (red dot approx. location of side control actuator)

Fig. 9   SCW load arm *x*-direction deflection (in.) at maximum applied load in brake-roll condition based on nonlinear analysis (from Ref. [9]).
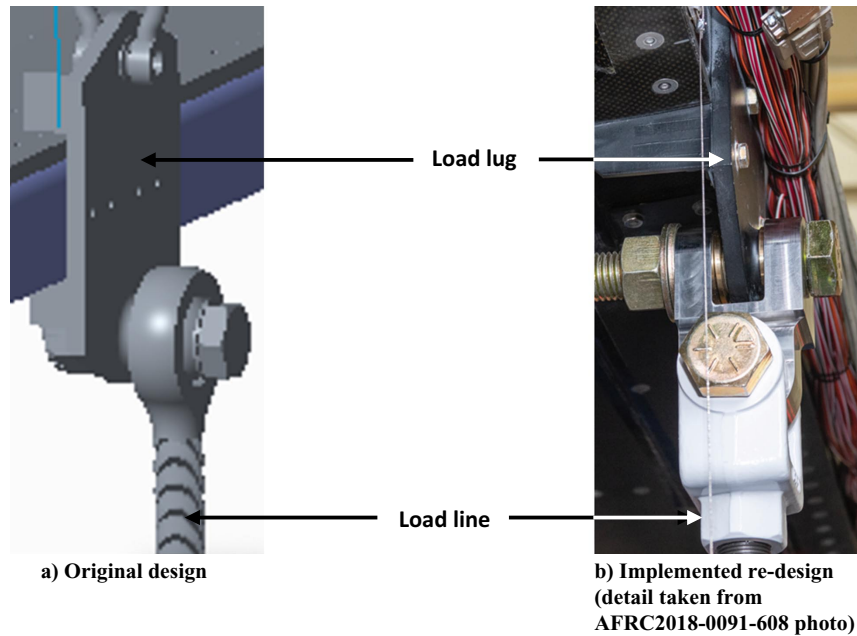
Fig. 10   PAT wing lug load-introduction modification to relieve lug stresses.

Lesson 1) *Analyze the test configuration using appropriate analysis approaches.*

While tests to determine whether a design satisfies the loading requirements are planned to apply loads consistent with the way the loads would be applied in the flight vehicle, the test configuration does not always meet that goal. Additionally, details of the fixture design may lead to loads that are eccentric and those eccentricities must be taken into account in the analysis models. Therefore, while analysis of the actual in-service loading scenario is necessary for designing structures, analysis of the actual test setup including the test fixture hardware, eccentricities, and load orientation is necessary to adequately design the test and predict the test response. Lastly, analysis approaches should be appropriate to accurately predict the response, such as using nonlinear analysis when nonlinear response may be present due to large deformations or eccentric loads. One way to ensure that the modeling approaches are appropriate is to review past analyses as the design progresses. Deficiencies in the preliminary analyses for the PAT wing were identified by the first author while reviewing the analyses and how the results were used in the design process. Conducting periodic reviews of modeling approaches is made easier by utilizing a modeling and analysis plan (MAP) as was done during SBKF [10]. As stated in the reference, the objective of the SBKF MAP was "to provide a uniform guideline on how to develop and execute the SBKF analysis tasks, and to provide a means by which assumptions, modeling techniques, and other information pertinent to the tasks are identified, documented, and archived in a complete and consistent way." Having such an organized set of models and analysis data makes evaluation of assumptions, and determination of appropriateness, significantly easier and traceable.

B.   Lesson 2: Load-Introduction Structure Response

The second lesson learned is associated with the response of the load-introduction structure. The lesson is exemplified by the PAT wing test and the SBKF 8 ft metallic barrel tests that used self-reacting loading structures, and the full-scale 27.5-ft-diam metallic barrel tests that used heritage hardware. Assumptions are typically made during test analyses about the boundary conditions and stiffnesses of load-introduction structure, often with boundary conditions assumed on the test article with the load-introduction structure ignored (not modeled). The aforementioned tests had load-introduction structures that exhibited both rigid-body motions and/or elastic deformation during testing. Because of the possibility of these deformations, digital image correlation (DIC) data and conventional data, including rotations measured with inclinometers or displacement measurements at numerous locations, were

collected from the load-introduction structure, and that data enabled identification of several load-introduction structure responses that led to test and analysis correlation discrepancies. During PAT wing testing, the reaction table, pedestal, and the structure connecting the reaction table to the pedestal exhibited both rigid-body motions and elastic deformations. These rigid-body motions and elastic deformations within the self-reacting structure introduced global deflection components that resulted in significant errors in the wing deflection response measurement in the PAT wing testing. By considering the DIC and conventional data collected, rigid body and elastic responses of the load-introduction structure could be characterized and used to improve test and analysis correlation by correcting the measured deflection data from the wing. Figure 11 shows the vertical (z-direction) deflection response for the inboard 250-in. portion of the wing at two different load levels for the up-bending load condition [11], where the test data are from DIC measurements made using the markers at the LE and TE as seen in Fig. 2. The test results were adjusted to remove the effect of the rigid body motion of the PAT wing resulting from the compliance of the load-introduction structure (designated with "ADJ" in the name), where the designations in the adjusted results indicate that the rigid body rotation was calculated by the two side DIC systems (DIC Component), from a virtual inclinometer derived from the top DIC system (DIC Top System), or from the traditional inclinometer mounted on the top cover of the wing near the root (Inclinometer). The DIC Top System and Inclinometer measurements are direct wing rotation measurements from the top skin, while the DIC component was an attempt to determine wing rotation using rotations of the individual components of the load-introduction system. The test and analysis correlation errors in the PAT wing vertical deflection response were reduced from about 19 to 4% on the inboard portion of the wing by adjusting for the rigid body motion of the PAT wing, as shown in the figure.

In a similar manner, the upper spider and transition cylinder can exhibit rigid-body translations and rotations during the 8 ft metallic barrel tests. Test data from the 8 ft metallic barrels did identify small rigid-body motions that were not predicted in the high-fidelity FEM, but these motions had little influence on the test article responses of interest (strains, axial displacement, and local deformations). Lastly, during the initial full-scale metallic barrel test sequences, the attachment ring region at the intersection of the test article with the load-introduction simulators was observed to be rotating about the local tangent direction, which resulted in a poor end shortening test and analysis correlation because axial measurements were taken by displacement transducers attached to these rings. A means of measuring those rotations was implemented that utilized pairs of displacement
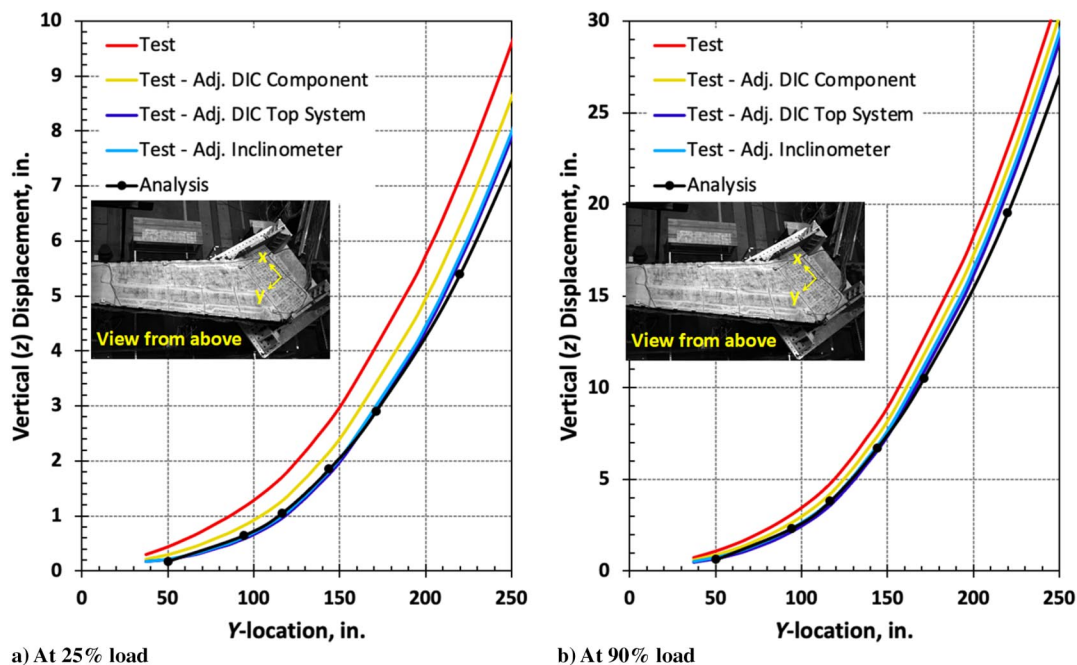
a) At 25% load   b) At 90% load

Fig. 11 PAT wing inboard-250-in.-portion trailing edge vertical (z) displacement at 25 and 90% of $2.5g$ up-bending load (adapted from Ref. [11]).

transducers at each location and enabled adjustment of the axial measurements to improve the end-shortening test and analysis correlation [3]. Therefore, the following is the second lesson learned:

Lesson 2) *Characterization of load-introduction structure response is critical to understanding test response.*
Assumptions about the boundary conditions, including load-introduction structure, in an analysis can influence predicted responses, lead to deficiencies in the test design, and lead to poor test and analysis correlation. Characterization of the load-introduction structure is necessary to verify if the modeling assumptions associated with the load-introduction structure were accurate. Errors associated with boundary condition assumptions can be particularly important in self-reacting systems, such as those discussed herein, that can exhibit rigid-body motion in addition to elastic response, but similar response can also be seen with test stands that can have "settling" upon the introduction of load as well as deformations of the test stand. Instrumenting load-introduction structure can provide data that can enable identification of unexpected load-introduction response that can then be used to improve test and analysis correlation and the design of future tests. For test setups that are connected to rigid structure (ground), elastic response of the load-introduction structure may occur and should be characterized. Consideration may be particularly important when using heritage hardware and where full details of the as-built hardware are not available, as was the case for the full-scale metallic barrel tests, which makes accurate modeling of these structures difficult. Therefore, it is also advisable to conduct tests on heritage load-introduction structure to characterize its performance whenever possible to help inform modeling of the heritage structure in test modeling.

C. Lesson 3: Load-Application System

The third lesson learned is associated with the applied loads on a test article. In the case of the PAT wing, as mentioned in Sec. II.A, the inboard pairs of load lines, where the deflections were smaller, were mounted so that the loads at maximum load were applied normal to the wing. However, because of the large wing tip deflections that were expected during the PAT wing up-bending test, an alternate approach was used to apply the three pairs of loads on the outboard part of the wing. For the outer sets of load lines, pairs 5, 6, and 7, AFRC test engineers developed a unique overhead loading structure as shown in Figs. 2 and 3. The loads applied using the overhead structure were split with I-beam spreader bars at each of the three load line locations into a pair or loads in a whiffle tree configuration. The overhead

loading assembly included three load actuators to pull the three load cables, combined with three pully position control actuators that changed the position of the cable pullies in the overhead structure. Moving the cable pullies changed the position where the load cables were effectively connected in the overhead structure, thus changing the orientation of the applied load as needed. The ability to move the load cable connection point in the overhead structure allows the load to be applied normal to the wing throughout the loading sequence, and it is a very effective approach to control load application orientation and simulate the actual aerodynamic loads on the structure throughout the entire load application. However, the overhead load structure was designed very early in the project due to scheduling constraints.

When the overhead load structure for the PAT wing test was designed, the predicted displacements were significantly smaller than those eventually observed during the test, and those smaller predicted displacements were used to size the actuator strokes. Also, the motion of the pulley toward the wing root during loading generated additional slack in the line because the distance that the load cable had to traverse from the actuator, over the pulley, and down to the spreader bars was shortened. This shortening of the cable distance created the need for additional stroke of the load application actuator, and this additional stroke was accounted for in the initial design with the initial stroke requirements. Unfortunately, the test article exhibited much larger displacements than expected due to flexibility of the boundary (as described in Lesson 2) and the test article being much more flexible than originally predicted. The larger displacements exhibited by the test article required more pulley motion and, therefore, more pulley and load actuator stroke. However, because the overhead loading fixture was designed and constructed before identification of the increased deflections, the additional needed stroke, combined with the geometry of the overhead load structure, led to insufficient stroke in the pulley and load actuators. Therefore, maintaining a normal load orientation at maximum load and throughout loading was not possible. Rather, the load vector rotated from an inboard orientation (acute angle between load vector and upper cover surface inboard of load application point) to an outboard orientation (obtuse angle between load vector and upper cover surface inboard of load application point) as depicted in Fig. 12. In the figure, the light blue lines represent the desired orientations with the loads being normal to the wing before loading and at the maximum load (and remaining normal throughout loading). To obtain the most normal load at the maximum loads, the pulleys were moved toward the wing
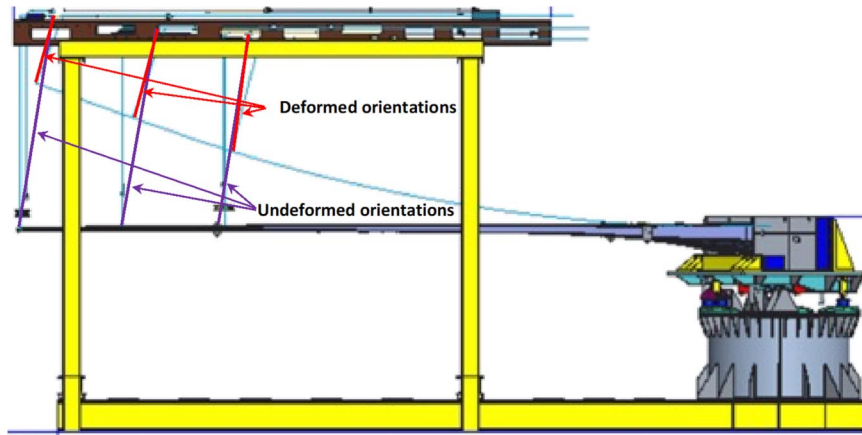
Fig. 12   PAT wing upper loading structure cable orientations for undeformed (purple lines) and deformed (red lines) configurations. Note: blue lines represent the originally desired normal load orientations.

root as much as possible within their stroke capabilities and fixed at that location throughout loading. The purple lines depict the orientations of the loads that were set up for the final test with the pulley positions fixed at maximum inward position, and the red lines depict the orientations of the loads at maximum loading with the pulley positions fixed at maximum inward position. Based on this test experience, the following is the third lesson learned:

Lesson 3) *Design the load application structure with sufficient margin to account for variability in test article predicted response.* Whether for conventional load lines on the stitched wing and inboard on the PAT wing, or the moving overhead load application system used outboard on the PAT wing, capability limits of the test setup should significantly exceed the predicted load and stroke required. That is, significant margin should be applied to the predicted limits of the test article response to ensure that the test setup does not preclude attaining the required test loads and deflections. In the case of the overhead structure, the stroke for the load actuators should have had significant margin to account for possible underestimation of wing deflection and cable slack created by movement of the pulleys. This margin is especially important if the test design is done early in the project, as happened with the PAT wing, and/or with limited information. In cases such as this, an additional margin in stroke capability of 50% would not have been unreasonable and would have permitted sufficient stroke to attain the desired load orientation for the PAT wing test. Similarly, if a buckling test was being developed, then the load capability of the test system should be capable of applying sufficiently large loads to accommodate the possibility that the buckling load is significantly underpredicted, with the applied margin value being commensurate with the confidence in the predicted value. Thus, additional margins applied to both stroke and load capabilities are recommended, and the amount of margin should be higher for test-system designs finalized earlier in the process and when test-article-predicted responses are more preliminary in nature. However, margins can be smaller for designs developed closer to the test and when test article responses are better understood. For example, a 13-ft-diam fluted-core sandwich barrel was produced for testing at the LaRC COLTS facility, where during manufacture the noodle region between the inner and outer skins and the fluted core segments were filled with unidirectional fibers rather than the expected matrix only noodle. As a result, the predicted buckling load increased by about 25%, which then exceeded the load capabilities of the COLTS facility. Therefore, for preliminary design it may be reasonable to design a system with 40–50% increased capability (displacement and load), while for detailed design cases capabilities should be 15–25% higher than expected.

D.   Lesson 4: Full-Field Response Measurement

The fourth lesson learned is associated with full-field response measurement, and is demonstrated by the MBB testing, where the test article contained thin skins and was subjected to compressive

loading. For the MBB structure, buckling was an important consideration. During testing of the MBB, portions of the test article exhibited different response under the same loading condition for different test cycles of that same loading condition. For example, the crown panel on the top of the test article exhibited local buckling of the skins between stiffeners for the up-bending condition that subjected the crown panel to compressive forces. Incorporating as-manufactured imperfections in the analysis has been shown to improve test and analysis correlation, as was seen for the SBKF project. However, as demonstrated by the MBB, even if the imperfections were known and easily incorporated in the predictive analysis, multiple postbuckled equilibria existed for localized responses due to slight variations in testing conditions. The out-of-plane deformation at design ultimate load (DUL) of the MBB crown panel under the 2.5-g up-bending loading, where the pattern is dominated by the inward (blue) and outward (red) local skin buckling between the stiffeners, is shown in Fig. 13. Results for two separate test cases, pristine and with barely visible impact damage (BVID), where BVID test cases include impacts with energy levels that result in damage that may be missed during a visual inspection, are shown in Fig. 13. As seen in the figure, different buckling patterns were obtained in the pristine and BVID test load sequences, while the finite element results predicted the same response for pristine and BVID. However, the localized BVID was not applied to the crown panel, and no appreciable effects of the multiple BVIDs were noted elsewhere in the far-field response. Therefore, the uniqueness of the deformation field for structures with multiple stable equilibria in their periodic features cannot be guaranteed, and a particular buckling pattern obtained in each test may likely be triggered by seemingly insignificant factors such as small manufacturing imperfections, scatter in the applied load path, or minor residual stresses from the previous tests and/or servicing of the test article between the tests. Several nonlinear finite element analyses were executed with slight changes to solver parameters, for example, the integration step increment, and those parameter changes also resulted in nonunique distinct buckling patterns [12]. The ability to develop a comprehensive understanding of the response might have been compromised if only a few strain gages were used to monitor the response. For example, if local skin buckling were to occur during the test in the direction opposite to the pretest prediction, the comparison of the test and analytical strain data would likely show a qualitatively inaccurate response correlation (tension instead of compression or vice versa). The inability to correctly characterize nonunique response in the test due to insufficient data could cause confusion when monitoring response during the test and/or during the post-test data analyses. Therefore, acquiring and monitoring full-field measurements should be incorporated during testing in order to understand response complexities associated with nonunique solutions. Similar necessity for full-field measurements was demonstrated by the examples in Lesson 2, where measurements of the complex boundary response consisting of rigid-body motion
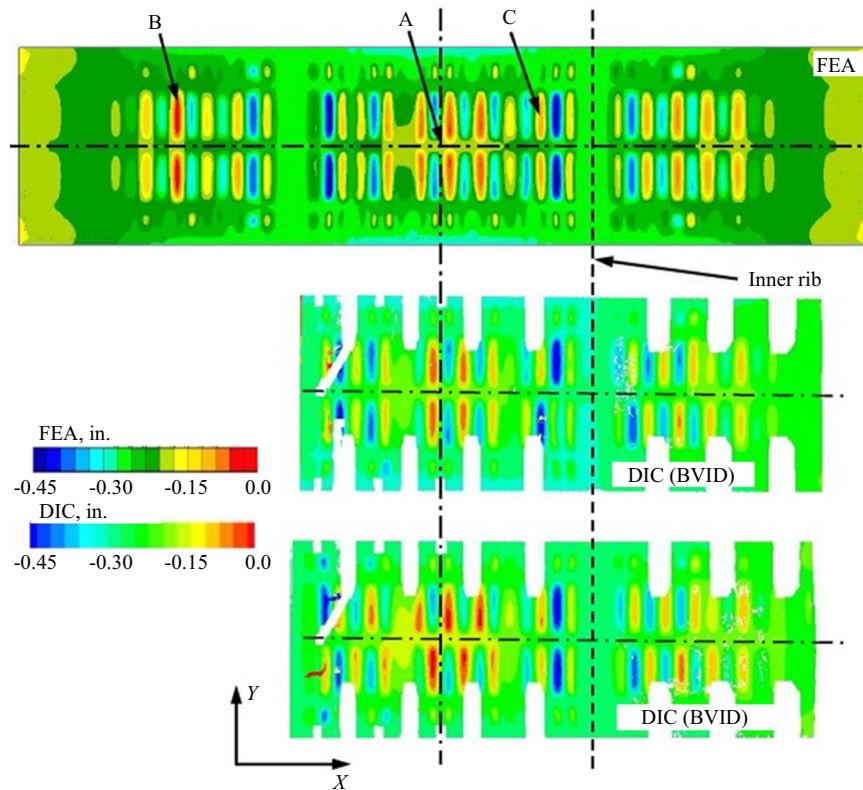
Fig. 13 Out-of-plane deformation (positive outward) of the MBB crown panel under 2.5*g* DUL (from Ref. [12]).

and elastic deformation were necessary. Such a capability can be accomplished using DIC as was used to obtain the test results shown in Fig. 13 and for the PAT wing boundary characterization of Lesson 2. Therefore, the following is the fourth lesson learned:

Lesson 4) *Full-field response measurements are crucial to understanding response when complex, and potentially nonunique, local (high-gradient) responses may occur.*
Because very small perturbations can result in changes in local buckling patterns, full-field measurements may be necessary to understand the actual local deformation for each loading cycle, particularly for thin-skin or thin-walled structures. Full-field measurements may also be necessary for buckling testing of a structure where there could be multiple global or local buckling modes with identical or very closely spaced eigenvalues to better identify the buckling pattern. In those cases where multiple local patterns may develop, the use of a limited number of conventional strain gages may not provide sufficient information to determine the response. Therefore, the use of full-field measurements provides robustness in the test data to account for uncertainties in the response of large-scale, complex structures.

E. Lesson 5: Residual Stresses

The fifth and final lesson learned presented herein is related to residual stresses and is demonstrated by the full-scale metallic barrel tests. As described in Sec. I.C, the full-scale barrels were formed by friction-stir welding eight panels that had been formed to 168 in. radius and then heat treated. Before welding, the panels were presumed to be in a stress-free state, that is, free from residual stresses due to manufacturing. However, the welding process resulted in local residual stresses at the welds and widespread residual stresses in the full barrel due to bending the panels together, i.e., decreasing their radius, to form the 165.5 in. radius of the test article. The residual stresses due to bending of the panels were particularly significant in the circumferential stiffeners, and those residual stresses ranged from small tension in the skin to a compressive maximum at the top edge of the stiffeners as a result of the weld-forming process [3]. Including residual stresses in finite element analysis had a small benefit on global response test and analysis correlation such as load/end-shortening curves, global

buckling, and strains. However, including the residual stresses showed significant improvement in local responses. The radial displacement contours for ETTA1 at 795 kip axial load and 1.0 psi internal pressure for the test, the baseline analysis, and an analysis including residual stresses are shown in Fig. 14 from work that was a continuation of Ref. [3]. The contour shapes and magnitudes are observed to have much better local deformation agreement between the test and the residual stress model results compared to the poor agreement between test and baseline model, particularly for skin pocket deformations in the vicinity of the panel centers and also within the weld lands. In fact, the predicted maximum inward (negative) deflection for the analysis with included residual stresses is within 1% of the measured test maximum inward deflection, which can be compared to 13% difference between the maximum inward deflections of the test and predicted with the baseline model. The improvement from 13 to 1% results from the improved skin pocket deflection prediction that was influenced by the residual stresses. Additionally, including the residual stress improved the test and analysis correlation for the deflections at the weld lands. That is, the difference in the maximum outward (positive) displacements between test and analysis is reduced to less than 14% error when the residual stresses are included in the finite element model, compared to the baseline model error of over 22%. Therefore, the following is the fifth lesson learned:

Lesson 5) *Residual stresses can have an effect on test article response, and should be included in the analysis whenever possible.* Understanding the manufacturing process for the test article and considering residual stresses in test articles is important because including residual stresses in the analysis can influence either global or local predicted responses, or both. Even though determining residual stresses in the test article may be difficult, these residual stresses should be included in analyses whenever possible to improve test and analysis correlation for test articles that have known residual stresses.

IV. Summary of Lessons Learned

Large-scale testing is an important part of research and development of aerospace structures. Representative aerospace structure tests are used to validate the performance of the structures or to provide
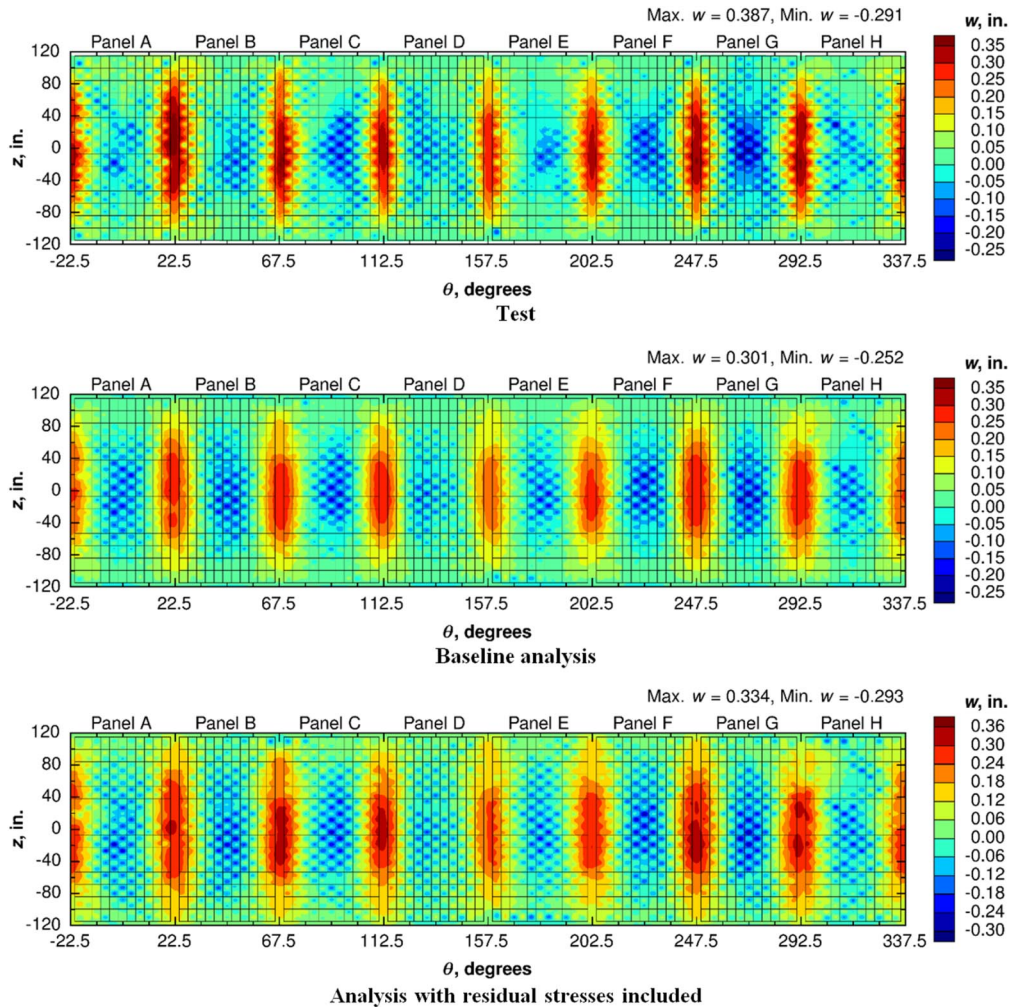
Fig. 14   ETTA1 radial displacement (in., positive outward) at 1.0 psi and 795-kip axial load.

full-scale response characteristics, quite often without having to resort to testing of a full-scale structure. However, due to the difficulties that can exist in conducting tests, such as representing correct boundary conditions and applying loads, there are certain lessons learned that need to be considered. Presented herein are five lessons learned from several large-scale tests conducted by researchers at LaRC. Lessons learned were as follows:

1) Analyze the test configuration using appropriate analysis approaches.

2) Characterization of load-introduction structure response is critical to understanding test response.

3) Design the load application structure with sufficient margin to account for variability in test article predicted response.

4) Full-field response measurements are crucial to understanding response when complex, and potentially nonunique, local (high-gradient) responses may occur.

5) Residual stresses can have an effect on test article response, and should be included in the analysis whenever possible.

Researchers and test engineers, from beginner to experienced, should remember these lessons learned when planning and conducting tests, and while performing test and analysis correlation. While many of these lessons may seem intuitive, they can often be ignored when schedule and cost become crucial aspects of a project when these lessons are not kept in mind at all times. Application of these lessons has eliminated potential failures of load-introduction hardware for the SCW and the PAT wing tests; enabled accurate test and analysis correlation for the PAT wing, the MBB, and the full-scale 27.5-ft and large-scale 8-ft metallic barrels tested; and enabled identification of limitations of the overhead load-introduction structure for the PAT wing tested. All of the large-scale test articles presented

herein, with the exception of the fluted-core test article that was not tested, were successfully tested due, in part, to understanding and applying these lessons learned. In general, failure to understand and apply these lessons may result in a test that is unable to obtain the desired data or test results, and therefore result in failure to meet project objectives. Engineers should always be vigilant and attempt to identify sources of potential uncertainties, such as the effects of modeling assumptions and the lack of knowledge of certain design aspects, when designing and analyzing large-scale structural tests. Tracking the appropriateness of the analyses can be made more rigorous and simplified if a modeling and analysis plan is incorporated into the testing effort in order to provide well-documented and configured models and analysis data to compare back to the actual test setup as it evolves.

References

[1] Jegley, D. C., Bush, H G., and Lovejoy, A. E., "Structural Response and Failure of a Full-Scale Stitched Graphite-Epoxy Wing," *Journal of Aircraft*, Vol. 40, No. 6, Nov.–Dec. 2003, pp. 1192–1199.
https://doi.org/10.2514/2.7209

[2] Jutte, C. V., Wiesemann, C. D., Lovejoy, A. E., and Stafford, B. K., "Static Loads Testing of a High Aspect Ratio Tow-Steered Wingbox," *AIAA SciTech 2020 Forum*, AIAA Paper 2020-0243, Jan. 2020.
https://doi.org/10.2514/6.2020-0243

[3] Lovejoy, A. E., Hilburger, M. W., and Gardner, N. W., "Test and Analysis of Full-Scale 27.5-Foot-Diameter Stiffened Metallic Launch Vehicle Cylinders," *2018 AIAA/ASCE/AHS/ASC Structures, Structural Dynamics, and Materials Conference*, AIAA Paper 2018-1989, Jan. 2018.
https://doi.org/10.2514/6.2018-1989

[4] Hilburger, M. W., Haynie, W. T., Lovejoy, A. E., Roberts, M. G., Norris, J. P., Waters, W. A., and Herring, H. M., "Subscale and Full-Scale Testing of Buckling-Critical Launch Vehicle Shell Structures," *53rd AIAA/ASME/ASCE/AHS/ASC Structures, Structural Dynamics and Materials Conference*, AIAA Paper 2012-1688, April 2012.
https://doi.org/10.2514/6.2012-1688

[5] Jegley, D. C., Rouse, M., Przekop, A., and Lovejoy, A. E., "The Behavior of a Stitched Composite Large-Scale Multi-Bay Pressure Box," NASA TM-2016-218972, April 2016.

[6] Vassberg, J. C., DeHaan, M. A., Rivers, S. M., and Wahls, R. A., "Development of a Common Research Model for Applied CFD Validation Studies," *26th AIAA Applied Aerodynamics Conference*, AIAA Paper 2008-6919, Aug. 2008.
https://doi.org/10.2514/6.2008-6919

[7] Brooks, T. R., Kenway, G. K. W., and Martins, J. R. R. A., "Benchmark Aerostructural Models for the Study of Transonic Aircraft Wings," *AIAA Journal*, Vol. 56, No. 7, 2018, pp. 2840–2855.
https://doi.org/10.2514/1.J056603

[8] Hilburger, M. W., Lovejoy, A. E., Thornburgh, R. P., and Rankin, C., "Design and Analysis of Subscale and Full-Scale Buckling-Critical Cylinders for Launch Vehicle Technology Development," *53rd AIAA/ASME/ASCE/AHS/ASC Structures, Structural Dynamics and Materials Conference*, AIAA Paper 2012-1865, April 2012.
https://doi.org/10.2514/6.2012-1865

[9] Lovejoy, A. E., "Finite Element Analysis of a Composite Semi-Span Test Article with and Without Discrete Damage," NASA CR-2000-210308, Aug. 2000.

[10] Lovejoy, A. E., and Hilburger, M. W., "SBKF Modeling and Analysis Plan: Buckling Analysis of Compression-Loaded Orthogrid and Isogrid Cylinders," NASA TM-2013-218037, Aug. 2013.

[11] Lovejoy, A. E., Gardner, N. W., Dawicke, D. S., Jutte, C. V., and Smith, B., "Improving Structural Test and Analysis Correlation Using Digital Image Correlation Boundary Measurements," *AIAA SciTech 2020 Forum*, AIAA Paper 2020-2188, Jan. 2020.
https://doi.org/10.2514/6.2020-2188

[12] Przekop, A., Jegley, D. C., Lovejoy, A. E., Rouse, M., and Wu, H.-Y., "Testing and Analysis of a Composite Non-Cylindrical Aircraft Fuselage Structure, Part I: Ultimate Design Loads," *57th AIAA/ASCE/AHS/ASC Structures, Structural Dynamics, and Materials Conference*, AIAA Paper 2016-2176, Jan. 2016.
https://doi.org/10.2514/6.2016-2176

P. Weaver
Associate Editor